Interplay between surface and bending energy helps membrane protrusion formation

Raj Kumar Sadhu [*] and Sakuntala Chatterjee

Department of Theoretical Sciences, S. N. Bose National Centre for Basic Sciences, Block JD, Sector III, Salt Lake, Kolkata 700106, India

We consider a one-dimensional elastic membrane, which is pushed by growing filaments. The filaments tend to grow by creating local protrusions in the membrane and this process has surface energy and bending energy costs. Although it is expected that with increasing surface tension and bending rigidity, it should become more difficult to create a protrusion, we find that for a fixed bending rigidity, as the surface tension increases, protrusions are more easily formed. This effect also gives rise to nontrivial dependence of membrane velocity on the surface tension, characterized by a dip and a peak. We explain this unusual phenomenon by studying in detail the interplay of the surface and the bending energy and show that this interplay is responsible for a qualitative shape change of the membrane, which gives rise to the above effect.

I. INTRODUCTION

Inside a cell, actin filaments grow and exert polymerization force on the plasma membrane and create membrane protrusions. This process plays an important role in cell motility [1–7]. In many experiments, it has been studied how the mechanical properties of the plasma membrane directly affect the formation of membrane protrusion. For example, by artificially increasing the membrane tension in experiments, it has been seen that the rate of protrusion formation goes down, while by decreasing the membrane tension, the rate is found to increase [8,9]. Although, these studies indicate that the membrane tension is generally an obstacle to protrusion formation, in [10], it was shown that in certain situations, membrane tension can also enhance protrusions by streamlining actin polymerization in one specific direction.

These studies show it is important to understand how the elastic interactions in the membrane influence the mechanism of protrusion formation and in this Rapid Communication, we address this question in a simple setting. We model the elastic membrane using the Helfrich Hamiltonian, which is the most commonly used model that includes surface and bending energy of the membrane [11–26]. We describe the membrane using a one-dimensional height field, whose time evolution is governed by the Helfrich Hamiltonian. Any variation in the height costs energy and a flat membrane corresponds to the lowest energy configuration. We consider the membrane being pushed by few growing filaments, which tend to create protrusions in the membrane that cost energy [27–30]. As surface tension σ or bending rigidity κ of the membrane is increased, one would expect that protrusion formation should become more difficult, since the energy cost for creating a protrusion ought to go up monotonically with σ and κ. Surprisingly, we find it is not so. For a fixed value of κ, there is a significant range of σ, for which the energy cost actually decreases with σ, which makes protrusion formation easier. More specifically, the surface energy cost for creating a local

protrusion in the membrane increases monotonically with σ, as expected, but the bending energy cost shows a peak, which in turn gives rise to a peak in the total energy cost. Not only for cell motility, our finding has potential implications for a wide class of systems, where elastic deformation of a membrane is involved. The fact that we have been able to observe this effect in a simple and general model is encouraging and this opens up the exciting possibility of finding it in many different kinds of systems.

To understand the mechanism behind this intriguing effect, we examine the shape of the membrane near the binding site, where the filament is in contact with the membrane, and show that a qualitative change in the shape is responsible for this. In Fig. 1, we depict this mechanism. In the limit when both σ and κ are large, the membrane has very slow spatial variation of its height. In this limit, one can neglect higher order derivatives of height and assume the height profile of a local protrusion is almost linear in space, as shown in Fig. 1 by the thin red line. For such a local shape of the membrane, the bending energy (which scales as the square of the second derivative of height) has a nonzero value at the binding site. Everywhere else on the membrane near the binding site, the bending energy is negligible. As σ decreases slightly but still remains large, the shape of the membrane remains qualitatively the same, but the height gradient magnitude now increases (see the blue dotted line in Fig. 1) and the bending energy becomes significantly larger at the binding site. To minimize this energy, as σ is lowered further, the membrane shape finally changes qualitatively, and becomes as shown by the black thick line in Fig. 1, where the peak gets rounded and the height profile also does not remain linear anymore. While the bending energy now is nonzero even away from the binding site, its variation across the membrane happens more gradually. The bending energy cost to create a local protrusion, which is proportional to the fourth derivative of height, is lower for such a configuration.

II. DESCRIPTION OF THE MODEL

Our system consists of a set of N parallel filaments growing against a membrane as shown in Fig. 2. The membrane is
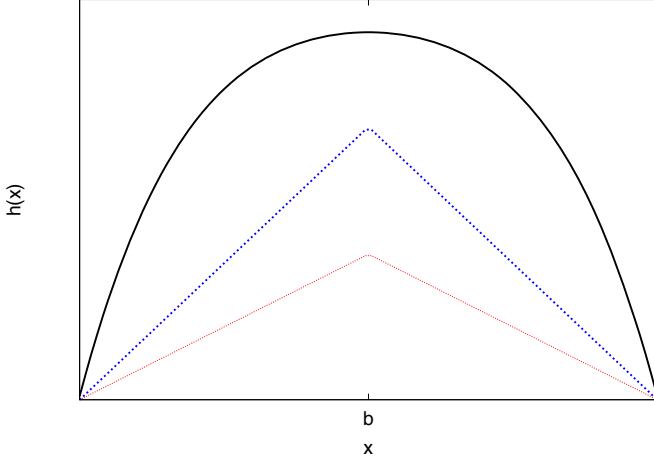
*rajkumar.sadhu@bose.res.in

020401-1

FIG. 1. Schematic picture of typical membrane shape $h(x)$ around the binding site at $x = b$. Keeping κ constant at a moderate or large value, as σ is varied, the membrane shape changes qualitatively. The curve at the bottom (top) is for the largest (smallest) σ value.

described by a height profile $\{h_i\}$, defined on a one-dimensional lattice of length L with lattice constant unity. We assume periodic boundary condition $h_i = h_{i+L}$ on the lattice. In the absence of any external force, the height profile of the membrane follows an equilibrium dynamics with the Helfrich Hamiltonian, which is standardly used to describe the height fluctuations of a plasma membrane [12,14–16]. This Hamiltonian consists of surface interaction and bending interaction of the membrane and in our lattice model, it has the form [29–32]

$$
\mathcal{H} = \sigma \sum_{i=1}^{L} (h_i')^2 + \kappa \sum_{i=1}^{L} (h_i'')^2 = \sigma \sum_{i=1}^{L} (h_i - h_{i-1})^2
$$
$$
+ \kappa \sum_{i=1}^{L} (h_{i-1} - 2h_i + h_{i+1})^2, \qquad (1)
$$

where σ is proportional to the surface tension and κ to the bending rigidity. Both of these parameters have dimensions of energy/length^2, as follows from the above equation. In Eq. (1), we have neglected the nonlinear terms, which can be justified if the magnitude of height gradient everywhere on the membrane is much less than unity [24,33,34]. The size of a typical eukaryotic cell is about a few tens of micrometers [35], which can be compared with the size of our membrane patch. The horizontal distance between two consecutive lattice sites in our model can be taken to be $1/L$ times the size of the membrane. The vertical height difference between two consecutive lattice sites is in the scale of nanometers, set by the size of an actin monomer. Thus, height gradient remains small and the linear approximation for the Hamiltonian in Eq. (1) remains valid.

It follows from Eq. (1) that the minimum energy configuration is reached when the membrane is completely flat, i.e., h_i the same for all i. For a finite temperature, the membrane undergoes thermal fluctuations, as a result of which h_i can increase or decrease by an amount δ. The corresponding
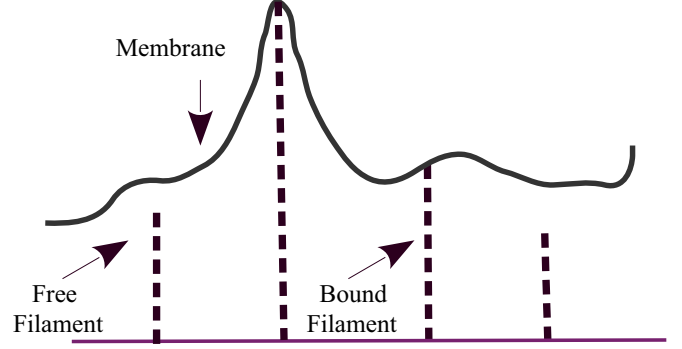

FIG. 2. Schematic diagram of the model. The thick solid line represents the height profile of the membrane and thick dashed lines represent the bound and free filaments.

energy costs $\mathcal{E}_i^{\pm}$ can be obtained from Eq. (1) as

$$
\mathcal{E}_i^{\pm} = \sigma\{2\delta^2 \mp 2\delta(h_{i-1} - 2h_i + h_{i+1})\} + \kappa\{6\delta^2 \pm 2\delta(h_{i-2}
$$
$$
- 4h_{i-1} + 6h_i - 4h_{i+1} + h_{i+2})\}
$$

or, in terms of the discrete derivatives,

$$
\mathcal{E}_i^{\pm} = \sigma\{2\delta^2 \mp 2\delta h_i''\} + \kappa\{6\delta^2 \pm 2\delta h_i''''\}
$$
$$
= \Sigma_i^{\pm} + \mathcal{K}_i^{\pm}. \qquad (2)
$$

Here $\mathcal{E}_i^{+}$ denotes the total energy cost for changing h_i to $h_i + \delta$ and Σ_i^{+} denotes the surface energy cost and $\mathcal{K}_i^{+}$ denotes the bending energy cost for the same process. Similarly, $\mathcal{E}_i^{-}$, Σ_i^{-}, and $\mathcal{K}_i^{-}$ are the respective energy costs for changing h_i to $h_i - \delta$. We use the Metropolis algorithm to perform the simulations.

One additional constraint that the system must obey is that the height of the membrane at the binding sites should be such that the membrane always stays above the filament tips (as shown in Fig. 2). Any height fluctuation that brings a binding site at a lower height than the filament tip, is forbidden. As long as this constraint is satisfied, the update rules can be chosen following the local detailed balance $R_+/R_- = e^{-\beta\epsilon}$, where R_+ is the rate of a process that has a positive energy cost ϵ and R_- is the rate of the reverse process.

The filaments are modeled as rigid rodlike polymers, composed of monomers of length d [27,36–38]. In Fig. 2, we have represented the filaments using dashed lines, each dash denoting a monomer. A (de)polymerization event increases (decreases) the length of a filament by an amount d. For the sake of simplicity, we have used $d = \delta$ here [also see Eq. (2)]. In Sec. VII of [39], we have included our data for the $d \neq \delta$ case. There are two types of filaments in our model: a free filament, which is not in contact with the membrane, and a bound filament, whose tip is in contact with the membrane site [27,36,37,40]. The point of contact is referred to as a binding site. For a free filament, polymerization happens with rate U_0. For a bound filament, however, a polymerization process increases the height of the binding site by an amount d and hence there is an energy cost involved in this process. For a positive (negative) energy cost, the bound filament polymerization rate is taken to be $U_0 R_+$ ($U_0 R_-$), while for zero energy cost, the rate is simply U_0. The depolymerization rate of the filament is equal to W_0 always, as it does not involve
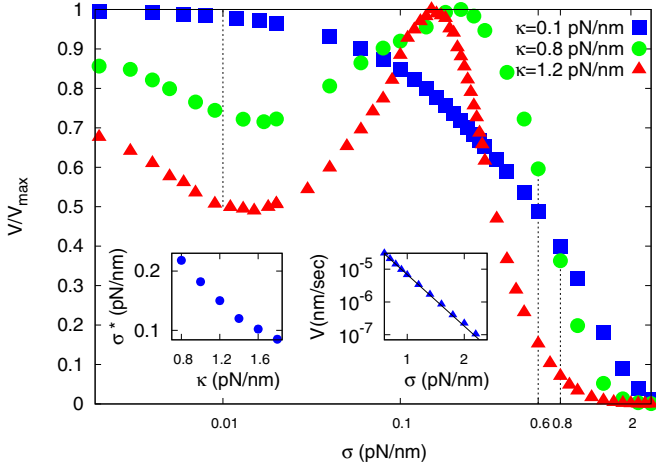
FIG. 3. σ-V curve for different values of κ. For small κ values, V decreases with σ, but for moderate or large κ values, V shows a minimum and a maximum. We scale each curve by V_{max}, which denotes the largest value of V for a particular V-σ curve. We have $V_{max} = 3.45 \times 10^{-2}$ nm/s, 1.55×10^{-3} nm/s, and 2.00×10^{-4} nm/s for $\kappa = 0.1$ pN/nm, 0.8 pN/nm, and 1.2 pN/nm, respectively. The vertical lines show σ values used in Fig. 5. Left inset: peak position σ^* shifts leftward with κ. Right inset: Exponential fall of V for large σ with $\kappa = 1.2$ pN/nm. The decay constant 3.6 matches closely with the analytical prediction $2\beta\delta^2$. Here, for all the plots, we use $L = 64$. The filament depolymerization rate, $W_0 = 1.4$ s^{-1} [1,40,41], the free filament polymerization rate, $U_0 = 2.784$ s^{-1} [1,40,41], the monomer size is $d = \delta = 2.7$ nm [1,40,42], $\beta = 1/k_B T$, and we have used $T = 300$ K.

any membrane movement. Note that, in the absence of any polymerization force from the filaments, the membrane tends to stay flat and this aspect is somewhat similar to lamellipodial protrusions, rather than filopodial protrusions observed in a cell. In our simulation, each Monte Carlo step consists of L membrane updates and N filament updates. The detailed simulation algorithm has been presented in Sec. I of [39].

III. RESULTS

We present our results in this section. As mentioned in the Introduction, our main result is the nonmonotonic variation of the membrane velocity as a function of σ. We first present our simulation data showing this effect and then we show how this nontrivial behavior can be explained from detailed measurement of the energy cost and the shape of the membrane. We show our results for a single filament ($N = 1$) here. Most of our conclusions remain valid even for the case of multiple filaments, if the filament density is not too high.

A. Membrane velocity shows a dip and a peak with σ

Pushed by the growing filaments, the membrane develops an average velocity. In Fig. 3, we present our data for the variation of membrane velocity V as a function of the surface tension σ, for a fixed value of bending rigidity κ. We find that for small κ, velocity decreases monotonically with σ, as expected [27]. However, as κ is held fixed at a moderate or large value, V shows a rich behavior: starting with a nonzero value at $\sigma = 0$, V first decreases with σ and reaches a minimum and
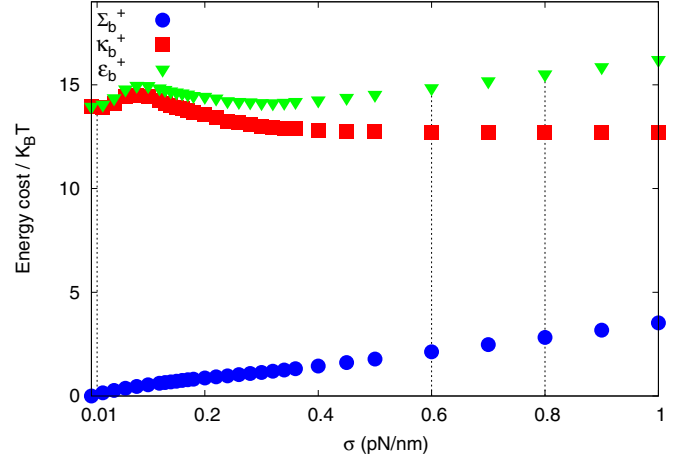

FIG. 4. Average energy cost for creating a protrusion at the binding site. Surface energy cost Σ_b^+ increases with σ but bending energy cost $\mathcal{K}_b^+$ shows a peak. For moderate or large κ values, when $\mathcal{K}_b^+$ is dominant, this gives rise to a peak in total energy cost $\mathcal{E}_b^+$. For very large σ, we see $\mathcal{K}_b^+$ saturating and variation in $\mathcal{E}_b^+$ is then controlled by Σ_b^+ again. These data are for $\kappa = 1.2$ pN/nm and the other simulation parameters are as in Fig. 3. The vertical lines correspond to σ values used in Fig. 5.

then it increases to reach a maximum before finally decreasing exponentially for large σ. While this nonmonotonic behavior is in general interesting [27], the most intriguing observation here is that, there is a range of σ for which V grows with σ. This growth is counterintuitive because one generally expects that with increasing surface tension, it should become more difficult for the filament to push the membrane. As we show in the following section, this expectation in fact breaks down.

The data in Fig. 3 is for a fixed L value. We have checked that as L is increased, $V \sim 1/L$, but the peak position does not depend on L for sufficiently large L values. As L becomes small, the peak in the V-σ plot shifts to lower σ values with decreasing L (Fig. S-5 of [39]).

B. Bending energy cost shows a peak with σ

From Eq. (2), it follows that the energy cost $\mathcal{E}_b^+$ for creating a protrusion at the binding site $i = b$ can be decomposed into two parts: the surface energy cost Σ_b^+ and the bending energy cost $\mathcal{K}_b^+$. In Fig. 4, we plot the steady-state average values of $\mathcal{E}_b^+$, Σ_b^+, and $\mathcal{K}_b^+$ as a function of σ, for a large value of κ. While Σ_b^+ increases with σ monotonically, $\mathcal{K}_b^+$ is found to show a peak. Moreover, this peak appears for relatively small σ values, when the total energy cost is actually controlled by the bending interaction. As a result, $\mathcal{E}_b^+$ also shows a peak and immediately after the peak, there is a range of σ values, for which energy cost decreases with σ, contrary to the normal intuition. Finally, for very large σ, when the membrane is almost flat, $\mathcal{K}_b^+$ saturates and Σ_b^+ increases linearly with σ [see Eq. (2)] and $\mathcal{E}_b^+$ also shows a linear rise.

Although, it seems quite surprising that energy cost shows nonmonotonic variation with σ, this effect can be very simply explained from the consideration of the membrane shape near the binding site. For very large σ and κ, the membrane remains almost flat and higher order derivatives of height can be ignored and one can assume an almost linear height
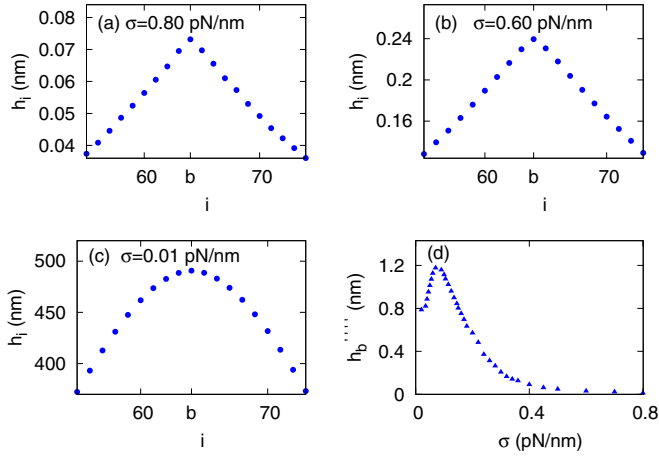
FIG. 5. (a)–(c) Local shape of the membrane around the binding site for different σ with $\kappa = 1.2$ pN/nm. (d) Discrete fourth derivative of height at the binding site, $h_b'''' = h_{b-2} - 4h_{b-1} + h_b - 4h_{b+1} + h_{b+2}$, as a function of σ. Here, $L = 64$ and the other simulation parameters are as in Fig. 3.

variation around the binding site. We check this explicitly in our simulations [see Fig. 5(a)]. Note that, here we only present the height profile near the binding site and far away from this point, height variation does not remain linear anymore, the profile gradually flattens out. However, this part of the membrane does not influence the energy cost near the binding site. In the region around the binding site, where height profile is linear, the bending energy, which depends on the second derivative of height, has a nonzero value only at the binding site, and zero elsewhere. Keeping κ fixed at large value, as we lower σ, the qualitative shape of the membrane remains similar, but the magnitude of the height gradient is now larger [Fig. 5(b)]. This, however, gives rise to a very high bending energy around the binding site, since height gradient changes sharply from a large positive value to a large negative value across the binding site. Therefore, as σ is lowered further, such a membrane shape becomes unsustainable and instead a shape shown in Fig. 5(c) is observed, where height gradient does not change so sharply but varies more slowly in space. Such a membrane shape stores less bending energy than the one with a linear height variation. In Sec. III of [39], we have also included an approximate analytical explanation of this effect, where we analytically calculated the membrane shape, adapting a simplified description outlined in [43].

With the above picture in mind, it is now easy to understand the variation of the fourth derivative of height (that determines the bending energy required to create a protrusion) at the binding site. In the configuration shown in Fig. 5(a), the second derivative has a negative value at the binding site and zero elsewhere in its neighborhood. As we lower σ, the configuration changes to what is shown in Fig. 5(b) and the magnitude of the second derivative at the binding site increases, i.e., the minimum in h_i'' is now sharper. This will increase its curvature, i.e., the fourth derivative at the binding site. However, as the membrane shape changes to Fig. 5(c) for even lower σ, h_i'' now has a nonzero (negative) value even some distance away from the binding site, since the height

profile is not linear anymore. Around the binding site, h_i'' now varies more gradually and while it still has a minimum at the binding site, the minimum is not as sharp. This corresponds to a lower curvature and the fourth derivative decreases in magnitude. We show this explicitly in Fig. 5(d).

However, when κ is small, the above effect is absent. Since the bending energy is actually responsible for the change in membrane shape and for small κ, the bending energy is just not significant enough to bring about this change. In this case, the membrane height profile around the binding site remains linear for all σ values and the fourth derivative falls monotonically with σ. As a result, energy cost and velocity varies monotonically with σ (see Figs. S-1 and S-3 in [39]).

C. A more quantitative explanation of the full V-σ curve

In the previous section, we have offered a simple qualitative explanation of how the energy cost for creating a protrusion shows a peak with σ, for large values of κ. This makes it plausible that V can also show a similar peak, since pushing the membrane upward becomes easier as σ is increased within a certain range. However, the net membrane velocity results from both upward and downward movements of the membrane and in this section, we present a more quantitative and detailed calculation, that explains the full V-σ curve, along with its maximum and minimum.

The membrane being in steady state, its average velocity should be the same at all sites and below, we write down the expression for velocity at the binding site b. For large κ, height gradients at the binding site are small and hence energy costs $\mathcal{E}_b^{\pm}$ are positive [also see Eq. (2)], which gives

$$V_b = \delta[U_0 p_0 e^{-\beta \mathcal{E}_b^+} + e^{-\beta \mathcal{E}_b^+} - (1-p_0)e^{-\beta \mathcal{E}_b^-}], \quad (3)$$

where p_0 is the contact probability of the filament tip with the membrane. The first term in Eq. (3) corresponds to the bound filament polymerization. The second and third terms represent thermal fluctuation of the membrane height at the binding site. Here, we have used the fact that h_b can always increase with rate $e^{-\beta \mathcal{E}_b^+}$, but it can decrease only when the filament is not bound to the membrane.

As explained in Eq. (2), $\mathcal{E}_b^+$ ($\mathcal{E}_b^-$) is the energy cost for increasing (decreasing) h_b by an amount δ, and generally it depends on the local configuration around the binding site. Here, we use the approximation that $\mathcal{E}_b^{\pm}$ may be replaced by their average values (to keep our notations simpler, we have used the same symbol for the average quantities as well). We have also checked that (data not shown here) as long as κ is not too small, the contact probability p_0 does not show much variation and remains close to $1/2$, its value for a rigid barrier [27].

For large κ and small σ, the surface energy cost is much smaller than the bending energy cost and we can replace $\mathcal{E}_b^{\pm} \approx \mathcal{K}_b^{\pm}$ and this gives

$$V \approx e^{-6\beta\delta^2\kappa} \delta\{(U_0 + 1)p_0 e^{-2\beta\delta\kappa h_b''''}$$
$$- 2(1-p_0)\sinh(2\beta\delta\kappa h_b'''')\}. \quad (4)$$

It is easy to see from the above expression that as h_b'''' first increases with σ, reaches a peak, and then decreases, V also initially decreases with σ, reaches a minimum, and then

starts increasing. As σ increases further, it is not possible to neglect the elastic energy anymore and Eq. (4) does not remain valid. However, in this case, both σ and κ are large, and the magnitudes of h_b'' and h_b'''' are negligible, and we can write

$$V \simeq \delta(U_0 + 1)p_0 e^{-6\beta\delta^2\kappa} e^{-2\beta\delta^2\sigma}, \qquad (5)$$

where V decreases exponentially with σ. We verify this from our numerical simulation (Fig. 3, right inset). The exponential decay constant numerically observed is 3.6, which is close to the analytically predicted value $2\beta\delta^2 \simeq 3.52$. When κ is held fixed at a larger value, the exponential decay in Eq. (5) starts at a smaller value of σ, since the height derivatives become negligible already. This is why the peak position σ^* shifts toward smaller values as κ increases (Fig. 3, left inset).

IV. DISCUSSIONS

Throughout this Rapid Communication, we have limited our studies to one dimension and it is an important question whether our conclusions remain valid for a two-dimensional membrane as well. Generalizing Eqs. (1) and (2) for the two-dimensional case, it can be shown that the bending energy cost is much higher in this case, which slows down the time evolution for moderate or high values of κ. Although, for small κ values, we have been able to verify (data not shown here) that V decreases monotonically with σ, as found in the one-dimensional system, higher κ values remain numerically inaccessible to us. More research is needed to conclude with certainty if nonmonotonic variation of V with σ for high κ values persists in the two-dimensional model as well.

It should be possible to experimentally verify our conclusions. One direct measurement would be to measure the membrane velocity for different values of σ and κ [44–46] and see whether a non-monotonicity as shown in Fig. 3 can be found. The energy scales involved in our simulations are actually comparable to physical systems. For example, the increase of V with σ that we observe for high κ, corresponds to the surface energy varying in the range of 0.5–2 (10^{-19} J) and the bending energy lies in between 1 and 3.5 (10^{-19} J). These values are within the experimentally observed ranges for flexible membranes [47]. Although, in real systems, many other factors, apart from surface energy-bending energy interplay, are relevant, it would be interesting to see whether this basic signature of a protrusion formation mechanism can still be found.

[1] J. Howard, *Mechanics of motor proteins and the cytoskeleton* (Sinauer Associates, Sunderland, MA, 2001).

[2] T. D. Pollard and J. A. Cooper, Actin, a central player in cell shape and movement, Science **326**, 1208 (2009).

[3] L. Blanchoin, R. B. Paterski, C. Sykes, and J. Plastino, Actin dynamics, architecture and mechanics in cell motility, Physiol. Rev. **94**, 235 (2014).

[4] P. Friedl and D. Gilmour, Collective cell migration in morphogenesis, regeneration and cancer, Nat. Rev. Mol. Cell Biol. **10**, 445 (2009).

[5] J. Plastino and C. Sykes, The actin slingshot, Curr. Opin. Cell Biol. **17**, 62 (2005).

[6] B. Farrell, F. Qian, A. Kolomeisky, B. Anvari, and W. E. Brownell, Measuring forces at the leading edge: A force assay for cell motility, Integr. Biol. **5**, 204 (2013).

[7] X. Banquy, G. W. Greene, B. Zappone, A. B. Kolomeisky, and J. N. Israelachvili, Dynamics of force generation by confined actin filaments, Soft Matter **9**, 2389 (2013).

[8] N. C. Gauthier, M. A. Fardin, P. Roca-Cusachs, and M. P. Sheetz, Temporary increase in plasma membrane tension coordinates the activation of exocytosis and contraction during cell spreading, Proc. Natl. Acad. Sci. USA **108**, 14467 (2011).

[9] D. Raucher and M. P. Sheetz, Cell spreading and lamellipodial extension rate is regulated by membrane tension, J. Cell Biol. **148**, 127 (2000).

[10] E. L. Batchelder, G. Hollopeter, C. Campillo, X. Mezanges, E. M. Jorgensen, P. Nassoy, P. Sens, and J. Plastino, Membrane tension regulates motility by controlling lamellipodium organization, Proc. Natl. Acad. Sci. USA **108**, 11429 (2011).

[11] W. Helfrich, Elastic properties of lipid bilayers: Theory and possible experiments, Z. Naturforsch C **28**, 693 (1973).

[12] L. C. L. Lin, N. Gov, and F. L. H. Brown, Nonequilibrium membrane fluctuations driven by active proteins, J. Chem. Phys. **124**, 074903 (2006).

[13] B. Peleg, A. Disanza, G. Scita, and N. Gov, Propagating cell-membrane waves driven by curved activators of actin polymerization, PLoS One **6**, e18635 (2011).

[14] S. Mark, R. Shlomovitz, N. S. Gov, M. Poujade, E. G. Mongrain, and P. Silberzan, Physical model of the dynamic instability in an expanding cell culture, Biophys. J. **98**, 361 (2010).

[15] E. B. Isaac, U. Manor, B. Kachar, A. Yochelis, and N. S. Gov, Linking actin networks and cell membrane via a reaction-diffusion-elastic description of nonlinear filopodia initiation, Phys. Rev. E **88**, 022718 (2013).

[16] R. Shlomovitz, N. S. Gov, and A. Roux, Membrane-mediated interactions and the dynamics of dynamin oligomers on membrane tubes, New. J. Phys. **13**, 065008 (2011).

[17] J. Weichsel and P. L. Geissler, The more the tubular: Dynamic bundling of actin filaments for membrane tube formation, PLoS Comput. Biol. **12**, e1004982 (2016).

[18] L. C. L. Lin and F. L. H. Brown, Dynamic simulations of membranes with cytoskeletal interactions, Phys. Rev. E **72**, 011910 (2005).

[19] J. Daillant, E. B. Amalric, A. Braslau, T. Charitat, G. Fragneto, F. Graner, S. Mora, F. Rieutord, and B. Stidder, Structure and fluctuations of a single floating lipid bilayer, Proc. Natl. Acad. Sci. USA **102**, 11639 (2005).

[20] F. Quemeneur, J. K. Sigurdsson, M. Renner, P. J. Atzberger, P. Bassereau, and D. Lacoste, Shape matters in protein mobility within membranes, Proc. Natl. Acad. Sci. USA **111**, 5083 (2014).

[21] G. V. Bossa, B. K. Berntson, and S. May, Curvature Elasticity of the Electric Double Layer, Phys. Rev. Lett. **120**, 215502 (2018).

[22] J. B. Fournier, Dynamics of the Force Exchanged between Membrane Inclusions, Phys. Rev. Lett. **112**, 128101 (2014).

[23] M. Lenz, D. J. G. Crow, and J. F. Joanny, Membrane Buckling Induced by Curved Filaments, Phys. Rev. Lett. **103**, 038101 (2009).

[24] A. Veksler and N. S. Gov, Phase transitions of the coupled membrane-cytoskeleton modify cellular shape, Biophys. J. **93**, 3798 (2007).

[25] A. Veksler and N. S. Gov, Calcium-actin waves and oscillations of cellular membranes, Biophys. J. **97**, 1558 (2009).

[26] G. Orly, M. Naoz, and N. S. Gov, Physical model for the geometry of actin-based cellular protrusions, Biophys. J. **107**, 576 (2014).

[27] R. K. Sadhu and S. Chatterjee, Actin filaments growing against an elastic membrane: Effect of membrane tension, Phys. Rev. E **97**, 032408 (2018).

[28] S. L. Narasimhan and A. Baumgaertner, Dynamics of a driven surface, J. Chem. Phys. **133**, 034702 (2010).

[29] A. Baumgaertner, Crawling of a driven adherent membrane, J. Chem. Phys. **137**, 144906 (2012).

[30] R. Lipowsky and S. Grotehans, Renormalization of hydration forces by collective protrusion modes, Biophys. Chem. **49**, 27 (1994); Hydration vs. protrusion forces between lipid bilayers, Europhys. Lett. **23**, 599 (1993).

[31] A. Volmer, U. Seifert, and R. Lipowsky, Critical behavior of interacting surfaces with tension, Eur. Phys. J. B **5**, 811 (1998).

[32] D. Nelson, T. Piran, and S. Weinberg, *Statistical mechanics of membranes and surfaces* (World Scientific, Singapore, 2004).

[33] D. Kabaso, R. Shlomovitz, K. Schloen, T. Stradal, and N. S. Gov, Theoretical model for cellular shapes driven by protrusive and adhesive forces, PLoS Comput. Biol. **7**, e1001127 (2011).

[34] N. S. Gov and A. Gopinathan, Dynamics of membranes driven by actin polymerization, Biophys. J. **90**, 454 (2006).

[35] S. R. Bolsover, J. S. Hyams, E. A. Shephard, H. A. White, and C. G. Wiedemann, *Cell biology: A short course* (Wiley, Hoboken, NJ, 2004).

[36] R. K. Sadhu and S. Chatterjee, Actin filaments growing against a barrier with fluctuating shape, Phys. Rev. E **93**, 062414 (2016).

[37] R. K. Sadhu and S. Chatterjee, Actin filaments pushing against a membrane: Comparison between two force generation mechanisms, Eur. Phys. J. E **42**, 15 (2019).

[38] X. Li and A. B. Kolomeisky, The role of multifilament structures and lateral interactions in dynamics of cytoskeleton proteins and assemblies, J. Phys. Chem. B **119**, 4653 (2015).

[39] See Supplemental Material at http://link.aps.org/supplemental/10.1103/PhysRevE.100.020401 for details of simulation technique, shape of the membrane for small κ, analytical calculation of the membrane shape, κ-V curves for different σ, results for faster (slower) barrier dynamics, results for different membrane size (L), and results for the case $d > \delta$.

[40] K. Tsekouras, D. Lacoste, K. Mallick, and J. F. Joanny, Condensation of actin filaments pushing against a barrier, New J. Phys. **13**, 103032 (2011).

[41] T. D. Pollard, Rate constants for the reactions of ATP- and ADP-actin with the ends of actin filaments, J. Cell. Biol. **103**, 2747 (1986).

[42] D. K. Hansda, S. Sen, and R. Padinhateeri, Branching influences force-velocity curve and length fluctuations in actin networks, Phys. Rev. E **90**, 062718 (2014).

[43] R. Shlomovitz and N. S. Gov, Membrane Waves Driven by Actin and Myosin, Phys. Rev. Lett. **98**, 168103 (2007); Exciting cytoskeleton-membrane waves, Phys. Rev. E **78**, 041911 (2008).

[44] Y. Marcy, J. Prost, M. F. Carlier, and C. Sykes, Forces generated during actin-based propulsion: A direct measurement by micromanipulation, Proc. Natl. Acad. Sci. USA **101**, 5992 (2004).

[45] C. Brangbour, O. du Roure, E. Helfer, D. Démoulin, A. Mazurier, M. Fermigier, M. F. Carlier, J. Bibette, and J. Baudry, Force-velocity measurements of a few growing actin filaments, PLoS Biol. **9**, e1000613 (2011).

[46] S. H. Parekh, O. Chaudhuri, J. A. Theriot, and D. A. Fletcher, Loading history determines the velocity of actin-network growth, Nat. Cell Biol. **7**, 1219 (2005).

[47] R. Dimova, Recent developments in the field of bending rigidity measurements on membranes, Adv. Colloid Interface Sci. **208**, 225 (2014).

Correction: The Supplemental Material and the corresponding description in Ref. [39] have been revised.